Front. Earth Sci. 2023, 17(4): 905–919
https://doi.org/10.1007/s11707-022-1084-0

RESEARCH ARTICLE

# A re-evaluation of the average chain length of lacustrine sedimentary *n*-alkanes as a paleoproxy on the Qinghai-Tibet Plateau

**Mingda WANG (✉)[1,2,3], Qin LI (✉)[1], Jaime TONEY[3], David HENDERSON[3], Juzhi HOU[2,4]**

1 School of Geography, Liaoning Normal University, Dalian 116029, China
2 Alpine Paleoecology and Human Adaptation (ALPHA) Group, State Key Laboratory of Tibetan Plateau Earth System, Resources and Environment, Institute of Tibetan Plateau Research, Chinese Academy of Sciences, Beijing 100101, China
3 School of Geographical and Earth Sciences, University of Glasgow, Glasgow G12 8QQ, Scotland, UK
4 CAS Center for Excellence in Tibetan Plateau Earth Sciences, Beijing 100101, China



**Abstract** Long-chain *n*-alkanes are one of the most common organic compounds in terrestrial plants and they are well-preserved in various geological archives. *n*-alkanes are relatively resistant to degradation and thus they can provide high-fidelity records of past vegetation and climate changes. Nevertheless, previous studies have shown that the interpretation of *n*-alkane proxies, such as the average chain length (ACL), is often ambiguous since this proxy depends on more than one variable. Both vegetation and climate could exert controls on the *n*-alkane ACL, and hence its interpretation requires careful consideration, especially in regions like the Qinghai-Tibet Plateau (QTP) where topography, biome type and moisture source are highly variable. To further evaluate the influences of vegetation and climate on the ACL in high-elevation lakes, we examined the *n*-alkane distributions of the surface sediments of 55 lakes across the QTP. Our results show that the ACL across a climatic gradient is significantly affected by precipitation, rather than by temperature. The positive correlation between ACL and precipitation may be because of the effect of microbial degradation during deposition. Finally, we suggest that more caution is needed in the interpretation of ACL data in different regions.

**Keywords** ACL, average chain length, *n*-alkanes, leaf wax, lake sediments, Qinghai-Tibet Plateau

Received August 13, 2022; accepted May 18, 2023

E-mails: mdwang@lnnu.edu.cn (Mingda WANG)
liqin@lnnu.edu.cn (Qin LI)

## 1 Introduction

Rapid climate changes are especially evident in high mountain regions (Liu et al., 2009; Mountain Research Initiative EDW Working Group, 2015), such as the Qinghai-Tibet Plateau (QTP). As the largest and most important "water tower" in Asia, the QTP is experiencing rapid and unprecedented warming (Immerzeel et al., 2010; Immerzeel et al., 2020). Consequently, the water availability and the regional ecosystems are likely to be increasingly affected by this warming (Yao et al., 2019). Therefore, it is important to achieve a comprehensive understanding of past climate changes in such high-elevation regions and their potential effects on different types of water resource, which necessitates an improved understanding of the natural climate variability of these regions and the assessment of anthropogenic effects.

Sedimentary long-chain *n*-alkanes are often regarded as terrestrial higher plant biomarkers and their distributions and isotopic signatures are commonly used to reconstruct changes in continental climatic conditions and vegetation (Brincat et al., 2000; Zhou et al., 2005; Castañeda et al., 2009b; Sachse et al., 2012), for the following reasons. 1) As one of the major components of leaf waxes (Eglinton and Hamilton, 1967), *n*-alkanes are widespread and well-preserved in different sedimentary deposits (Diefendorf et al., 2011); and 2) plants can adapt to environmental stresses via the modification of the acyl chain, such as the biosynthesis of longer chain-length waxes to limit water loss (Shepherd and Wynne Griffiths, 2006, Tipple and Pagani, 2013). Due to their high relative abundance and additional characteristic source information, the *n*-alkane average chain length (ACL) has been used to infer past climatic and vegetation changes (Chen et al., 2020; Toney

et al., 2020; Xie et al., 2020). ACL can be interpretated in different ways, but it typically characterizes the relative contribution of different organic matters in the sediments when targeting a wide carbon range of ACL values (Norström et al., 2014; Jin et al., 2016; Günther et al., 2016; Witt et al., 2016; Saini et al., 2017; Callegaro et al., 2018; Yan et al., 2020). It is also regarded as a paleoproxy if the long-chain homologs are selected (Pu et al., 2013; Ling et al., 2017b; Liu et al., 2021).

During the past decade, the long-chain *n*-alkane ACL has been used for continental vegetation reconstruction (Zhou et al., 2012; Castañeda et al., 2016; Norström et al., 2017; Norström et al., 2018; Häggi et al., 2019). With the development of new proxies, various biomarker approaches have been used to reveal vegetation histories, such as lignin phenols ratios (Castañeda et al., 2009b), and the stable carbon isotope ratios of *n*-alkanes and lignin phenols (Huang et al., 1999a, 1999b; Feakins et al., 2005; Castañeda et al., 2009a; Sinninghe Damsté et al., 2011; Kuechler et al., 2013; Garcin et al., 2014); however, the analysis of *n*-alkane distributions is relatively straightforward. In some cases, the ACL proxy may complement other approaches used to reconstruct vegetation changes, such as the ratio of grasses to woody plants (Norström et al., 2018). The ACL can also be used to infer past climatic variability in natural archives, including marine sediments (Poynter et al., 1989; Li et al., 2015), lake sediments (Castañeda et al., 2009b; Pu et al., 2013; Sun et al., 2018; Tian et al., 2019), peat sediments (Nichols et al., 2006; Zhou et al., 2010; Zhang et al., 2014; Naafs et al., 2019), and loess-paleosol sequences (Zhang et al., 2006; Bai et al., 2009; Zech et al., 2013). However, several studies have revealed that the factors determining *n*-alkane distributions are not uniform (Schefuß et al., 2003; Bush and McInerney, 2015; Eley and Hren, 2018; Wang et al., 2018a).

For the Qinghai-Tibet Plateau, much effort has been expended to evaluate the impact of climatic variables on *n*-alkane average chain lengths; nevertheless, there is a debate about the interpretation of *n*-alkane ACL across the QTP. ACL was shown to respond to precipitation rather than to temperature, based on the analysis of lake surface sediments in the south-western QTP (Hu et al., 2014). Guo et al. (2015) investigated plants and surface soils in alpine meadow ecosystems across the eastern QTP and observed the effect of temperature on ACL. However, a study of soil samples by Jia et al. (2016) showed that both climatic variables (precipitation and temperature) were positively correlated with ACL. Although these studies have reported the relationships between ACL and climatic variables, a recent field experiment conducted in central Tibet concluded that neither temperature nor precipitation had a strong impact on the chain length of *n*-alkanes (Bai et al., 2019). Hence it is imperative to clarify whether ACL is an effective paleoproxy for lake sediments in this region.

To this end, we investigated the environmental factors determining the ACL in a series of surface sediments from 55 lakes across the QTP that were obtained during the past decade. Our specific objectives were to disentangle the influences of vegetation and climate on the long-chain *n*-alkane distributions, and to identify the main climatic variables that control the chain length of sedimentary *n*-alkanes in these lakes.

## 2 Materials and methods

### 2.1 Field sampling

Lake surface sediments from 55 lakes were collected during fieldwork between 2010 and 2017; 46 lakes are located along a west-east transect in Tibet, and 9 lakes are in the Qaidam Basin, an intermontane basin in the north-eastern QTP (Fig. 1(a), Table 1). The lake areas range from 6.3 $km^2$ (Zongxiong Co) to 2300.4 $km^2$ (Selin Co), and the altitudes range from 2689 m (Xitaijinaier) to 5086 m (Guozha Co) (Table 1). The 55 lakes span a relatively large climatic gradient, with the mean annual air temperature (MAAT) range from −6.9°C to 5.4°C and the mean annual precipitation (MAP) ranges from 44 mm to 635 mm (Figs. 1(b) and 1(c)). The main vegetation types around these lakes are meadow, steppe and desert (Hou, 2001). We collected the surface lake sediment samples (0–2 cm) using an Ekman-Birge grab, and immediately placed them in Nasco Whirl-Pak bags. In the laboratory, the samples were kept at −20°C prior to freeze-drying.

### 2.2 Lipid extraction and measurement

Approximately 2−4 g of freeze-dried lake surface sediments were ground and homogenized before lipid extraction. Samples were extracted using an accelerated solvent extractor system (Dionex ASE350) with dichloromethane (DCM): methanol (MeOH) (9:1, v:v), at the temperature and pressure of 120°C and 1500 psi, respectively. The total lipid extracts (TLEs) were quantified by comparing the weights of lipid extracts before and after drying under a stream of nitrogen gas using a TurboVap system. TLE were separated into neutral and acid fractions by elution through a LC-$NH_2$ SPE column using DCM:isopropyl alcohol (1:1, v:v), followed by ether with 4% acetic acid (v:v) as eluents, respectively. The neutral fractions were further separated into four fractions of increasing polarity via chromatography over a silica gel column using hexane, DCM, ethyl acetate:hexane (1:3, v:v) and MeOH as eluents.

*n*-Alkanes from the hexane fraction were detected and quantified using gas chromatography with a flame ionization detector (GC-FID). Samples were passed through the GC-FID (model Agilent 7890B) using GC

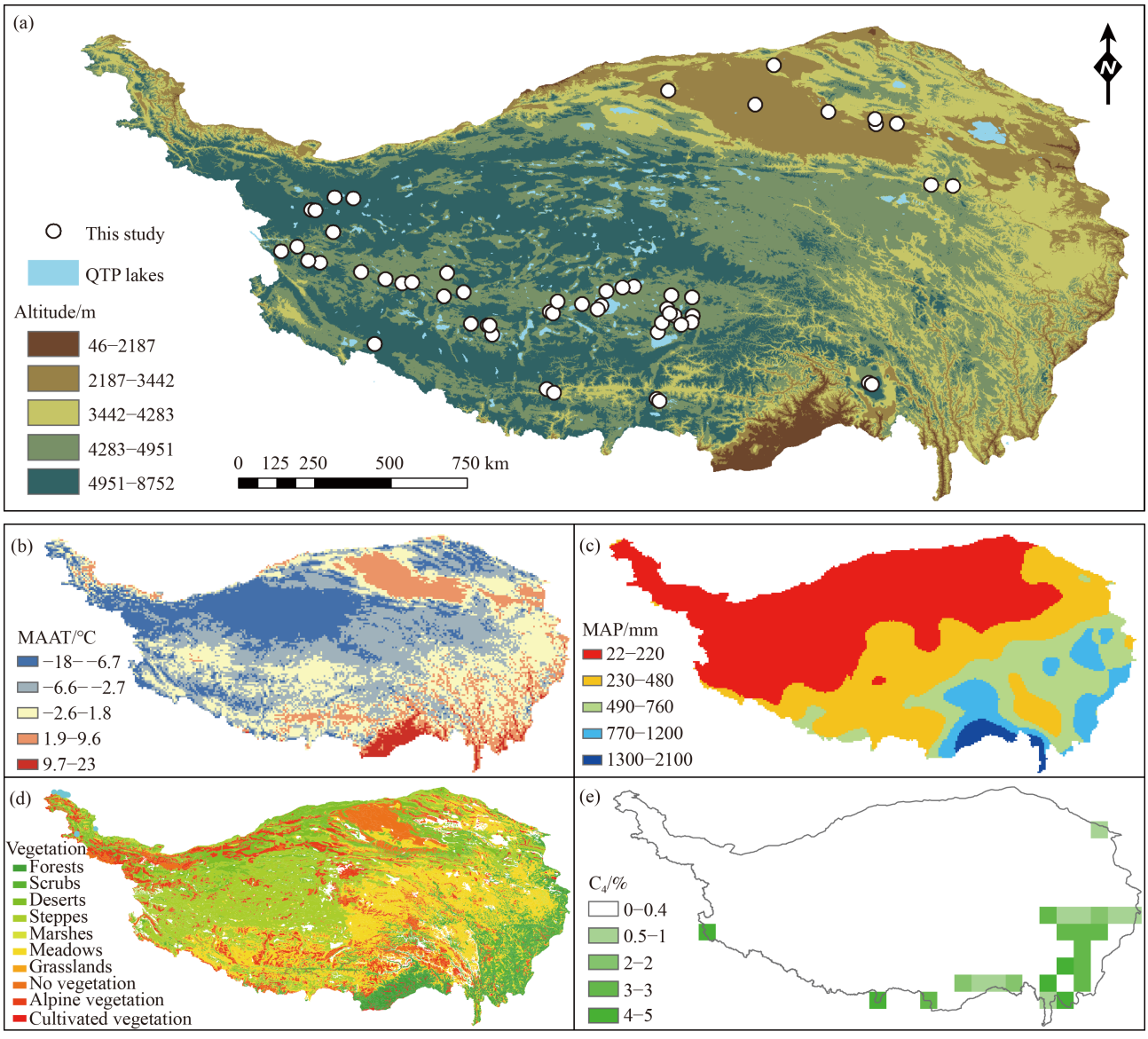


**Fig. 1** The study area and sampling locations along the two transects on the Qinghai-Tibet Plateau (QTP) (a) Gridded climate data are presented for both Mean Annual Air Temperature (MAAT). (b) and Mean Annual Precipitation (MAP). (c) Maps of vegetation information including biomes and the percentage of $C_4$ plants, respectively (d, e).

**Table 1** Sediment sampling site information

| No. | Lake | Latitude/°N | Longitude/°E | Elevation/m | Lake area/ km$^2$ | Salinity/(g·L$^{-1}$) | pH | MAAT/°C | MAP/mm | Vegetation zone |
|---|---|---|---|---|---|---|---|---|---|---|
| 1 | Shen Co | 30.9983 | 90.4792 | 4734 | 52 | 9.26 | 9.73 | −1.45 | 350 | steppe |
| 2 | Guozha Co | 34.9791 | 80.9386 | 5086 | 245 | 2.98 | 9.20 | −6.93 | 44 | desert |
| 3 | Bamu Co | 31.2634 | 90.5895 | 4565 | 255 | 7.51 | 9.70 | −0.87 | 350 | steppe |
| 4 | Gahai | 37.1404 | 97.5304 | 2852 | 35 | 76–94* | 8.40 | 4.73 | 197 | desert |
| 5 | Zigetang Co | 32.0729 | 90.8625 | 4573 | 238 | 13.5 | 10.00 | −1.38 | 372 | steppe |
| 6 | Rena Co | 32.7328 | 84.2545 | 4599 | 21 | 15.2 | 9.25 | −0.83 | 131 | steppe |
| 7 | Xiaochaidan | 37.4964 | 95.5019 | 3177 | 88 | 50* | 8.30 | 2.29 | 88 | desert |
| 8 | Bangong Co | 33.5171 | 79.8252 | 4244 | 671 | 0.47 | 8.73 | −0.59 | 88 | desert |
| 9 | Yangnapeng Co | 32.3409 | 89.7726 | 4634 | 17 | 30 | 9.92 | −0.57 | 285 | steppe |
| 10 | Cuoe-2 | 31.4606 | 91.4999 | 4528 | 85 | 3.63 | 9.51 | −1.30 | 394 | meadow |
| 11 | Bieruoze Co | 32.4304 | 82.9228 | 4407 | 36 | 27.38 | 8.97 | 1.47 | 131 | steppe |

(*continued*)

| No. | Lake | Latitude/°N | Longitude/°E | Elevation/m | Lake area/ km$^2$ | Salinity/(g·L$^{-1}$) | pH | MAAT/°C | MAP/mm | Vegetation zone |
|---|---|---|---|---|---|---|---|---|---|---|
| 12 | Gemang Co | 31.5825 | 87.2822 | 4610 | 62 | 6.35 | 9.73 | −1.25 | 219 | steppe |
| 13 | Dasugan | 38.8740 | 93.9036 | 2796 | 108 | 20 | 8.90 | 1.77 | 44 | desert |
| 14 | Bangda Co | 34.9420 | 81.4888 | 4909 | 143 | 35.11 | 8.50 | −5.53 | 44 | desert |
| 15 | Anggu Co | 31.1997 | 85.4482 | 4665 | 33 | 1.89 | 9.10 | −2.35 | 197 | steppe |
| 16 | Jieze Chaka | 33.9417 | 80.8814 | 4530 | 114 | 146* | 9* | −1.64 | 66 | desert-steppe |
| 17 | Nairiping Co | 31.2821 | 91.4713 | 4529 | 93 | 7.96 | 9.98 | −1.22 | 394 | steppe |
| 18 | Lagor Co | 32.0506 | 84.1696 | 4472 | 96 | 40.27 | 8.94 | −0.36 | 110 | steppe |
| 19 | Pusaier Co | 32.3147 | 89.4297 | 4593 | 34 | 5.3 | 9.66 | −0.06 | 263 | steppe |
| 20 | Aweng Co | 32.7695 | 81.7193 | 4430 | 70 | 27.65 | 9.20 | 1.63 | 131 | steppe |
| 21 | Dong Co | 32.1752 | 84.7392 | 4399 | 105 | 46.25 | 8.82 | −0.35 | 110 | steppe |
| 22 | Angrenjin Co | 29.3104 | 87.1997 | 4303 | 21 | 5.26 | 9.64 | 3.90 | 350 | steppe |
| 23 | Cuona | 32.0215 | 91.4819 | 4590 | 191 | 0.27 | 8.70 | −1.54 | 372 | meadow |
| 24 | Lang Co | 29.2068 | 87.4050 | 4296 | 10 | 1.58 | 9.44 | 4.57 | 329 | steppe |
| 25 | Zhangnai Co | 31.5467 | 87.3852 | 4611 | 44 | 4.06 | 9.60 | −1.13 | 241 | steppe |
| 26 | Peng Co | 31.4843 | 90.9576 | 4534 | 176 | 8.54 | 9.91 | −1.29 | 372 | steppe |
| 27 | Dawa Co | 31.2371 | 84.9667 | 4628 | 118 | 18.58 | 9.30 | −2.14 | 197 | steppe |
| 28 | Selin Co | 31.7675 | 88.7988 | 4544 | 2300 | 8.36 | 9.33 | 0.22 | 241 | steppe |
| 29 | Qiagui Co | 31.8153 | 88.2320 | 4558 | 89 | 0.22 | 8.83 | −0.11 | 241 | steppe |
| 30 | Kongmu Co | 29.0128 | 90.4394 | 4450 | 37 | 0.23 | 8.55 | 2.02 | 416 | steppe |
| 31 | Dongji Cona | 35.3334 | 98.5351 | 4086 | 241 | 0.35 | 8.76 | −2.30 | 219 | steppe |
| 32 | Daru Co | 31.6838 | 90.7440 | 4688 | 70 | 5.05 | 9.23 | −2.13 | 350 | steppe |
| 33 | Kuhai | 35.3054 | 99.1753 | 4132 | 47 | 16.1 | 8.82 | −2.89 | 263 | steppe |
| 34 | Beng Co | 31.2149 | 91.1654 | 4671 | 144 | 0.16 | 8.74 | −2.14 | 394 | steppe |
| 35 | Zhari Namco | 30.9136 | 85.5945 | 4617 | 1001 | 10.6 | 9.49 | −1.63 | 219 | steppe |
| 36 | Ga'a Co | 32.2090 | 88.9592 | 4620 | 13 | 3.38 | 9.68 | −0.44 | 241 | steppe |
| 37 | Xiada Co | 33.3888 | 79.3618 | 4358 | 8 | 0.15 | 8.60 | −2.29 | 110 | desert |
| 38 | Gasikule | 38.1209 | 90.7732 | 2857 | 116 | 333* | 7.50 | 2.31 | 66 | desert |
| 39 | Rebang Co | 33.0377 | 80.5138 | 4326 | 46 | 53.6 | 9.19 | −0.31 | 66 | desert |
| 40 | Xitaijinaier | 37.7175 | 93.3465 | 2689 | NIA | 336* | 7.7* | 3.99 | 44 | desert |
| 41 | Ranwu (AMC) | 29.4880 | 96.7010 | 3920 | 7 | 0.07* | 8.13* | 1.03 | 635 | Conifer forest |
| 42 | Ranwu (AC) | 29.4489 | 96.7921 | 3920 | 9 | 0.07* | 8.13* | 1.03 | 635 | Conifer forest |
| 43 | Zongxiong Co | 33.1032 | 80.1610 | 4351 | 6 | 0.15 | 9.34 | −1.49 | 66 | desert |
| 44 | Sumxi Co | 34.5997 | 80.2496 | 5057 | 31 | 0.26 | 8.53 | −5.86 | 44 | desert |
| 45 | Longmu Co | 34.5882 | 80.3677 | 5010 | 106 | 174* | 7.8* | −5.61 | 44 | desert |
| 46 | Zhacang Chaka | 32.5494 | 82.4297 | 4354 | 19 | 211* | 8* | 2.16 | 153 | steppe |
| 47 | Darebu Co | 32.4625 | 83.2161 | 4438 | 26 | 1.39 | 9.35 | 1.16 | 110 | steppe |
| 48 | Qige Co | 31.1957 | 85.5173 | 4667 | 20 | 0.18 | 10.46 | −2.38 | 175 | steppe |
| 49 | Cuoe-1 | 31.6655 | 88.7011 | 4568 | 268 | 0.21 | 8.84 | 0.11 | 241 | steppe |
| 50 | Chen Co | 28.9580 | 90.5174 | 4436 | 39 | 0.75 | 8.62 | 2.22 | 394 | steppe |
| 51 | Tuosu Lake | 37.1265 | 96.9176 | 2808 | 151 | 23.2 | 8.84 | 5.27 | 131 | desert |
| 52 | Hurleg Lake | 37.2868 | 96.8864 | 2817 | 55 | 0.66 | 8.49 | 5.39 | 131 | desert |
| 53 | Dagze Co | 31.8917 | 87.5235 | 4470 | 311 | 14.69 | 9.80 | 0.07 | 219 | steppe |
| 54 | Jiang Co | 31.5433 | 90.8179 | 4603 | 40 | 14.1 | 9.29 | −1.71 | 372 | steppe |
| 55 | Gongzhu Co | 30.6436 | 82.1090 | 4789 | 56 | 4.95 | 9.20 | −3.06 | 197 | steppe |

Notes: Source of data: 1) elevation: Google Earth Pro; 2) lake area: GaoFen-1 satellite, more details in Wan et al. (2016); 3) salinity and pH, in situ measurements; 4) temperature and precipitation: China meteorological forcing dataset (1979–2018); 5) vegetation zone: Hou (2001), vegetation zone in italic (Dr. Feng Qin. personal communication). An asterisk(*) is used to indicate the data from published papers, including Wang and Dou, (1998), Zhao et al. (2018), Liu et al. (2011), Ju et al. (2015), NIA=No Information Available.

column (Restek Rtx-1, 60 m × 0.25 mm id, 0.25 μm film thickness) for separation and then compared to an external standard (11 homologous series of *n*-alkanes from $C_{16}$ to $C_{37}$, CPAchem). The concentration of *n*-alkanes was calculated using the calibration curves of an external standard. The GC oven temperature program was as follows: initial temperature at 60°C, hold for 2 min, then ramp at 30°C/min to 120°C, and then ramp at 5°C/min to 330°C, hold at 330°C for 15 min.

In the present study, the ACL was calculated following Poynter et al. (1989), who first defined the metric ACL for the range of *n*-alkanes from $C_{23}$ to $C_{33}$. Later, this was refined by Poynter and Eglinton (1990) to target higher plants by employing only long-chain, odd *n*-alkanes. In the equation, $C_i$ = the peak area of *n*-alkanes containing *i* carbon atoms. We calculated the *n*-alkane ACL with different carbon ranges. Freeman and Pancost (2014) proposed that it was necessary to define the ACL with the molecule range in subscripts to avoid confusion; hence, it is important to carefully choose the carbon numbers for the calculations, which is necessary for assessing the impact of vegetation and climate on the *n*-alkane chain length. The other well-established *n*-alkane proxy, the Carbon Preference Index (CPI), was also calculated. In this study, we calculated the CPI values using the formula in Cooper and Bray (1963). ACL and CPI calculations with *n*-alkanes range from $C_{27}$ to $C_{33}$ are given below as examples:

$$ACL_{27\text{-}33} = \frac{(27\times C_{27} + 29\times C_{29} + 31\times C_{31} + 33\times C_{33})}{C_{27} + C_{29} + C_{31} + C_{33}}, \quad (1)$$

$$CPI_{27\text{-}33} = 1/2\left(\frac{C_{27} + C_{29} + C_{31} + C_{33}}{C_{26} + C_{28} + C_{30} + C_{32}} + \frac{C_{27} + C_{29} + C_{31} + C_{33}}{C_{28} + C_{30} + C_{32} + C_{34}}\right). \quad (2)$$

### 2.3 Climate estimates

Due to the sparse and inhomogeneous distribution of weather stations across the QTP, the meteorological observation data are limited, particularly for western Tibet. In this study, climate variables, including annual precipitation and temperature, were obtained from gridded climate data sets, namely the China Meteorological Forcing Data set (CMFD) (1979−2018) (He et al., 2020). The extracted temperature data represent the average value of a grid cell (with the spatial resolution of 0.1°), which requires calibration since there is an elevation difference between the location of the lake and the grid cell (Dr. Jie He, personal communication). The CMFD was developed by the Institute of Tibetan Plateau Research, Chinese Academy of Sciences, and the database has been widely utilized for climate studies throughout the QTP (Qiao et al., 2019; Wang et al., 2020). Recently, Wu et al. (2019b) compared three precipitation products for the QTP and concluded that the CMFD performed better than the others; hence, the CMFD product is the preferred gridded product for assessing climate data in this region.

### 2.4 Vegetation types

The dominant vegetation zones (biomes) were extracted from the Vegetation Atlas of China (Hou, 2001). In some cases, it is difficult to characterize the relatively complex vegetation cover in this region, which comprises diverse vegetation zones. Hence, GIS-based automated extractions and the literatures were both considered. The typical vegetation types in the catchments of the surveyed lakes include steppe, meadow and desert (Fig. 1(d)). We also extracted vegetation information in terms of photosynthetic composition, and the distribution of $C_4$ vegetation was provided from the ISLSCP II (International Satellite Land Surface Climatology Project) global data sets (Still et al., 2003, 2009) (Fig. 1(e)).

## 3 Results

### 3.1 Concentration of total lipid extracts

The total lipid extracts of the lake surface sediments, normalized to dry weight, generally vary between 1 mg/g and 15 mg/g with the average of 3.96 mg/g (Fig. 2). No significant differences were observed among lakes with contrasting salinity levels. The two highest TLE concentrations of the investigated lakes are Yanapeng Co (a mesosaline lake) and Darebu Co (a subsaline lake), with the values of 14.66 mg/g and 14.93 mg/g, respectively. Two lakes situated in western Kunlun (Sumxi Co and Guozha Co) and one proglacial lake (Ranwu Lake with three sub-basins, two of them are RW-AY and RW-AMC) in south-east Tibet had much lower TLE concentration (< 1 mg/g).

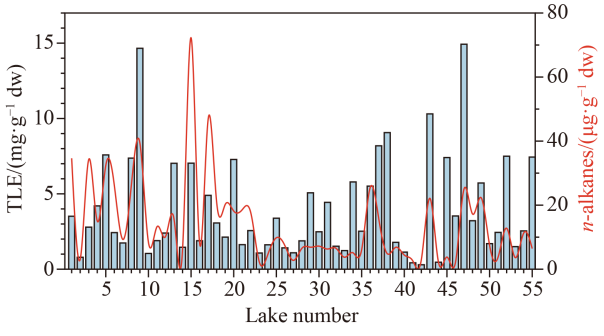


**Fig. 2** The concentrations of Total Lipid Extracts (TLEs) and *n*-alkanes from $C_{21}$ to $C_{35}$ (TLE in mg/g d.w., $\Sigma ALK_{21\text{-}35}$ in μg/g d.w.). The *x*-axis labels are consistent with the numbers in Table 1.

### 3.2 Distribution and concentration of *n*-alkanes

The surface sediments from the 55 lakes contain homologous series of *n*-alkanes between $C_{21}$ and $C_{37}$, albeit the homologs with the longest chain lengths ($C_{36}$ and $C_{37}$) are present at very low concentrations. Most of the samples showed strong odd/even predominance ($CPI_{27\text{-}33}$ values of these samples were generally > 5), except for the sample from Guozha Co ($CPI_{27\text{-}33}$ = 3.06). Marked differences in the *n*-alkanes distributions are evident, and four representative GC-FID chromatograms (Type I, Type II, Type III, and Type IV) are displayed in Fig. 3. Type I and Type II have a unimodal distribution with the dominant peaks $C_{29}/C_{31}$ and $C_{23}/C_{25}$, respectively. Type III is characterized by a bimodal distribution with maxima at $C_{23}/C_{25}$ and $C_{29}/C_{31}$. A distinctive *n*-alkane distribution pattern was observed for Dasugan Lake (Type IV), where the peak heights of the $C_{23}$, $C_{25}$, $C_{27}$, and $C_{29}$ *n*-alkanes were almost identical. The sum of the *n*-alkane concentrations (from $C_{21}$ to $C_{35}$) of the lake surface sediments varied significantly among the lakes, ranging from 2.11 μg/g to 72.26 μg/g (normalized to dry weight) with the average of 14.10 μg/g (Fig. 2). The summed concentrations of *n*-alkanes generally show similar spatial variations with the TLEs (Fig. 2). We calculated the *n*-alkane ACL values based on long-chain *n*-alkanes, but with different carbon ranges. For instance, $ACL_{27\text{-}31}$, $ACL_{27\text{-}33}$, and $ACL_{29\text{-}33}$ yielded the average values of 29.38 ± 0.37, 29.87 ± 0.38, and 30.57 ± 0.20, respectively.

## 4 Discussion

### 4.1 Sources of the long-chain *n*-alkanes

It is imperative to determine the specific sources of *n*-alkanes in sediments before using them as proxies for the reconstruction of paleovegetation and paleoclimate. There are two primary factors to be considered to elucidate the sources of recent sedimentary *n*-alkanes. One is the relative importance of aeolian and fluvial transport processes (McDuffee et al., 2004), and the other is the different biological sources of long-chain *n*-alkanes and their contributions.

#### 4.1.1 Aeolian versus fluvial transport

The leaf wax lipids are easily abraded from the plant leaf surface, and these lipids could be transported in air and deposited on the lake surface (Feakins et al., 2005). In addition, the aeolian transport of leaf wax lipids could occur via the erosion and redeposition of soil (Poynter et al., 1989; Kusch et al., 2010). Previous studies have demonstrated that aeolian dusts are the principal source of biological lipids of terrigenous materials in open ocean settings (Simoneit et al., 1977; Gagosian and Peltzer, 1986; Schefuß et al., 2003) and marginal seas (Wakeham, 1996; Yokoyama et al., 2006; Kusch et al., 2010). However, unlike the marine environment, the contribution of windblown *n*-alkanes to sediments could be quite different among lakes. Although several reviews have shown that the aeolian component was typically a small fraction of the total organic matter in lake sediments (Meyers and Ishiwatari, 1995; Meyers, 1997), several case studies have demonstrated that atmospheric deposition was an important mechanism for transporting waxes (Doskey, 2000; Hockun et al., 2016). Currently, there are few published data to evaluate the contribution of sedimentary *n*-alkanes for the lakes on the QTP. Here, we infer that the transport mechanism of the long-chain *n*-alkanes of the surveyed lakes is mainly associated with fluvial processes, via two mechanisms. 1) Lake ice prevents the atmospheric input of *n*-alkanes to the lake

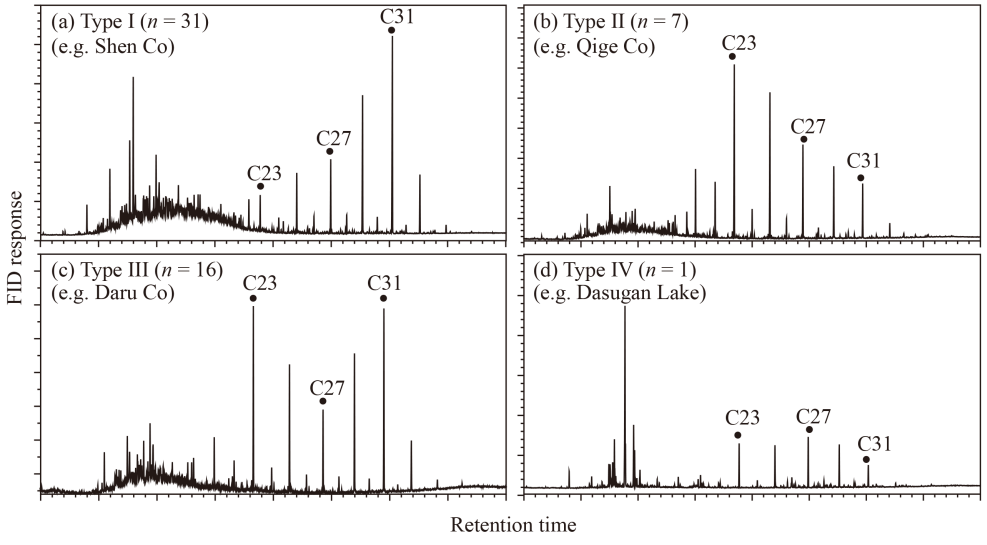


**Fig. 3** The four types of *n*-alkane distribution among the studied QTP lakes.

sediments during the windiest period of the year. Modern observations have shown strong winds prevail over the QTP from December to April, and the concentration of *n*-alkanes in total suspended particles is the highest at this time (Chen et al., 2014). However, ice phenology data revealed that a period of lake ice cover for most QTP lakes is from winter to spring (Wang et al., 2020); hence, the wind-blown *n*-alkane contribution to these lakes is probably minor. 2) Material sources available for transport during the ice-free season are not abundant. Atmospheric total suspended particle data in central Tibet and the south-eastern QTP showed that the lowest concentration of *n*-alkanes was in summer (Gong et al., 2011; Chen et al., 2014; Zhu et al., 2020). This evidence supports the assumption that contribution of airborne material to sedimentary *n*-alkanes is generally minor. However, we note that aeolian transport processes differ between lakes (Nelson et al., 2018), and further investigations are needed to quantitatively disentangle the organic matter contributions from different sources and transport mechanisms.

#### 4.1.2 Biological sources of long-chain *n*-alkanes

The chain length of the *n*-alkane homologs is usually from $C_{21}$ to $C_{37}$ in leaf waxes (Eglinton and Hamilton, 1967). ACL was first defined by Poynter et al. (1989), with the range from $C_{23}$ to $C_{33}$ *n*-alkanes, and it was later revised to $C_{27}$ to $C_{31}$ since this range is characteristic of terrestrial higher plants (Poynter and Eglinton, 1990). Recent studies have shown that submerged aquatic plants can also contribute to the sedimentary long chain *n*-alkanes (e.g., $C_{27}$ and $C_{29}$) of QTP lakes, particularly in the littoral zone (Aichner et al., 2010; Liu et al., 2015; Liu and Liu, 2016). We conducted a literature survey to determine if this was commonly the case for other lakes across the QTP. We addressed this issue by comparing the trends of variation in leaf-wax *n*-alkane $\delta$D values (*n*-$C_{27}$, *n*-$C_{29}$, and *n*-$C_{31}$) from a paleolimnological perspective. Although we found that the isotopic trends in *n*-$C_{27}$ were basically the same as in *n*-$C_{29}$ and *n*-$C_{31}$ over time (Bird et al., 2014; Rao et al., 2014; Günther et al., 2016), the correlation coefficients were only moderately high (*n*-$C_{27}$ vs. *n*-$C_{31}$, $R^2$ = 0.49–0.58), reflecting the mixed source of the $C_{27}$ *n*-alkane. In addition, we examined the potential sources of the $C_{27}$ *n*-alkane by applying principal component analysis to our data set. From Fig. 4 it is evident that the compound classes of *n*-alkanes are generally grouped into three clusters: Cluster 1 ($C_{21}$, $C_{23}$, $C_{25}$), Cluster 2 ($C_{27}$), and Cluster 3 ($C_{29}$, $C_{31}$, $C_{33}$, $C_{35}$). Therefore, the $C_{27}$ *n*-alkane likely has a mixed signal from terrestrial and aquatic plants, in agreement with previous studies.

### 4.2 Evaluation of vegetation influences on ACL

Previous studies have demonstrated that ACL responds to

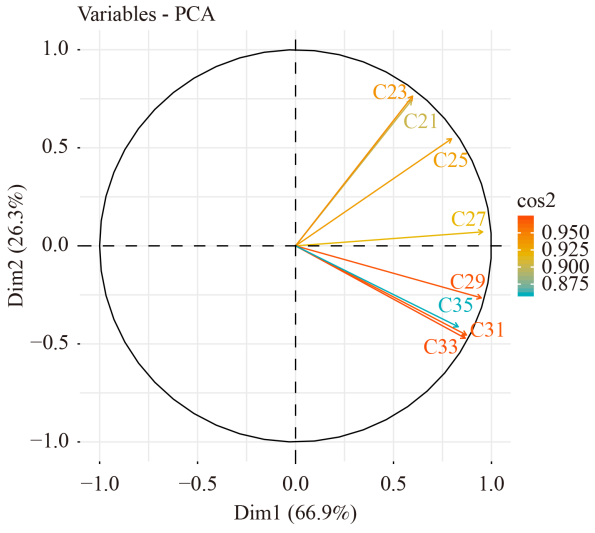


**Fig. 4** Results of principal components analysis (PCA). High cos2 indicates the strong loading of that variable on a given principal component, and vice versa.

variations in plant type (Vogts et al., 2009; Badewien et al., 2015) or climatic conditions (Castañeda et al., 2009b) in different environments; hence, caution is needed before interpreting the ACL data. Here, we aim to evaluate the influence of vegetation on the chain length of long-chain *n*-alkanes, and two types of information on plants were retrieved for reference: 1) life-forms such as trees, shrubs and grasses, and 2) different photosynthetic types such as $C_3$ and $C_4$ plants.

#### 4.2.1 Evaluation of vegetation influences on ACL from a plant life-form perspective

Many studies have shown that the ACL of *n*-alkanes varies between different plant types; for example, samples from grassland sites show systematically higher ACL values than those from deciduous trees/shrubs (Rommerskirchen et al., 2006; Vogts et al., 2009; Duan and He, 2011; Bliedtner et al., 2018). However, a meta-analysis of modern plants revealed no significant differences in chain length between grasses and woody plants (Bush and McInerney, 2013). Our previous study supported the conclusion of Bush and McInerney (2013) and concluded that the ACL could not distinguish graminoids from shrubs in some cases (Wang et al., 2015). For example, there were large overlaps between shrubs and grasses around Ranwu Lake in the south-eastern QTP, and similar observations are reported for other regions, like Australia (Howard et al., 2018) and Canada (Hollister et al., 2022).

For the sites in this study, the biome distribution was extracted from Vegetation Map of China (Hou, 2001). In addition, to extract plant life-form information, we also referred to the literature for verification (Wang and Dou, 1998; Qin, 2021). The dominant vegetation types for all

our sites are steppe, meadow and desert (Table 1). Trees are very sparsely distributed on the QTP due to the low temperatures and semi-dry to dry environment at high altitudes, resulting in a prevailing graminoid community with a few small shrubs in the lake catchments. Considering the large amount of overlap of the *n*-alkane chain length between grasses and shrubs, while grasses and shrubs were dominant compared to trees at the studied sites, the changes in ACL are unlikely to be caused by a shift in vegetation type, for example, from grasses to shrubs.

#### 4.2.2 Evaluation of vegetation influences on ACL from a photosynthetic perspective

Chain length, as well as carbon isotope composition, could distinguish $C_3$ from $C_4$ leaf wax *n*-alkanes, supported by the results obtained from modern plants (Rommerskirchen et al., 2006; Vogts et al., 2009), and hence ACL is deemed to be a good indicator of the spatiotemporal evolution of continental vegetation between the $C_3$ and $C_4$ photosynthetic pathways. Accordingly, it is widely used for paleovegetation reconstruction combined with compound specific stable carbon isotope analysis (Sarkar et al., 2015; Jalali et al., 2017).

Model simulations with a global distribution of $C_4$ mapping have shown that the modern $C_4$ plant species are very scarce at the study sites (Fig. 1(e)) (Still et al., 2003). Only a few field studies have reported that $C_4$ plants can survive in high-elevation environments (Wang, 2003; Wang et al., 2004). The scarcity of $C_4$ plants could be explained by the low temperature conditions in this high-elevation environment, regardless of precipitation (Rao et al., 2010). Therefore, the negligible distribution of $C_4$ plants at our study sites simplifies the interpretation of ACL from a photosynthetic perspective.

### 4.3 Evaluation of climatic influences on ACL

Plants can adapt to environmental stress by means of various physiologic mechanisms (Shepherd and Wynne Griffiths, 2006). Although ACL has been widely used as a paleoclimate proxy, its interpretations are ambiguous and region-specific. Transect studies have demonstrated the response of *n*-alkane ACL values to changes in hydrology (Hoffmann et al., 2013; Eley and Hren, 2018) and/or temperature (Tipple and Pagani, 2013; Bush and McInerney, 2015; Wang et al., 2018a). Accordingly, there are different interpretations of long-chain *n*-alkane ACL records. In paleolimnological studies in the QTP, ACL has been used to reconstruct past variations in effective humidity (Ling et al., 2017b; Zhang et al., 2017) or temperature (Pu et al., 2013; Ling et al., 2017a). Therefore, proxy calibrations in this region are needed to clarify its climatic implications and to reconcile the discrepancies between existing *n*-alkane ACL records.

The lakes surveyed in this study span a wide range of precipitation and temperature (Fig. 1), enabling us to assess the impact of these two climatic variables. Previous studies have suggested that precipitation and temperature usually exert opposing influences on the chain length of *n*-alkanes. A shift to longer chain homologs was found to be accompanied by lower precipitation (Carr et al., 2014; Eley and Hren, 2018) or higher temperatures (Leider et al., 2013; Tipple and Pagani, 2013; Bush and McInerney, 2015; Wang et al., 2018a). Our *n*-alkane data show that ACL is positively correlated with precipitation but it shows no relationship with temperature (Fig. 5), which is consistent with previous research on the QTP (Hu et al., 2014; Ling et al., 2021). However, such a positive correlation is contrary to the generally accepted understanding that land plants tend to synthesize longer *n*-alkane homologs in drier climatic conditions (Dodd and Afzal-Rafii, 2000; Dodd and Poveda, 2003). Hence, we now attempt to examine each of these two factors and to explain the observed relationships.

#### 4.3.1 Relationship between ACL and temperature

The proposed physiologic mechanism of the response of chain length to temperature is that plants increase the chain length to maintain their crystalline structure (Carr et al., 2014), or the so-called “hardness” of the leaf surface (Kawamura et al., 2003). The rationale behind is that compounds with longer carbon chains have slightly higher melting points, and their relative abundance in plants may be sufficient to maintain molecular alignment in the wax crystals under warmer condition (Gaines et al., 2009). Although numerous soil- and plant-based approaches have observed a close relationship between temperature and ACL (Tipple and Pagani, 2013; Bush and McInerney, 2015; Wang et al., 2018a, 2018b), no significant correlations were found for our data set (Fig. 5). To date, few studies have reported a positive response of *n*-alkane ACL values to temperature changes across the QTP, as evidenced by studies of modern plants and soils (Guo et al., 2015; Jia et al., 2016). Since all the samples in the present study are lake sediments, we ascribe this lack of a relationship between ACL and temperature to the complex processes of *n*-alkanes deposition in lakes. We also examined the temperature values extracted from CMFD and compared them with those of other studies. We found that the temperatures in our study were much lower and the gradient much smaller. For example, the temperature range was 20.2°C in Bush and McInerney (2015), which is almost twice as large as in our study. Hence the observed results could be partially explained by the temperature gradient, since the regression model showed a much greater scatter over a narrow temperature range (Bush and McInerney, 2015).

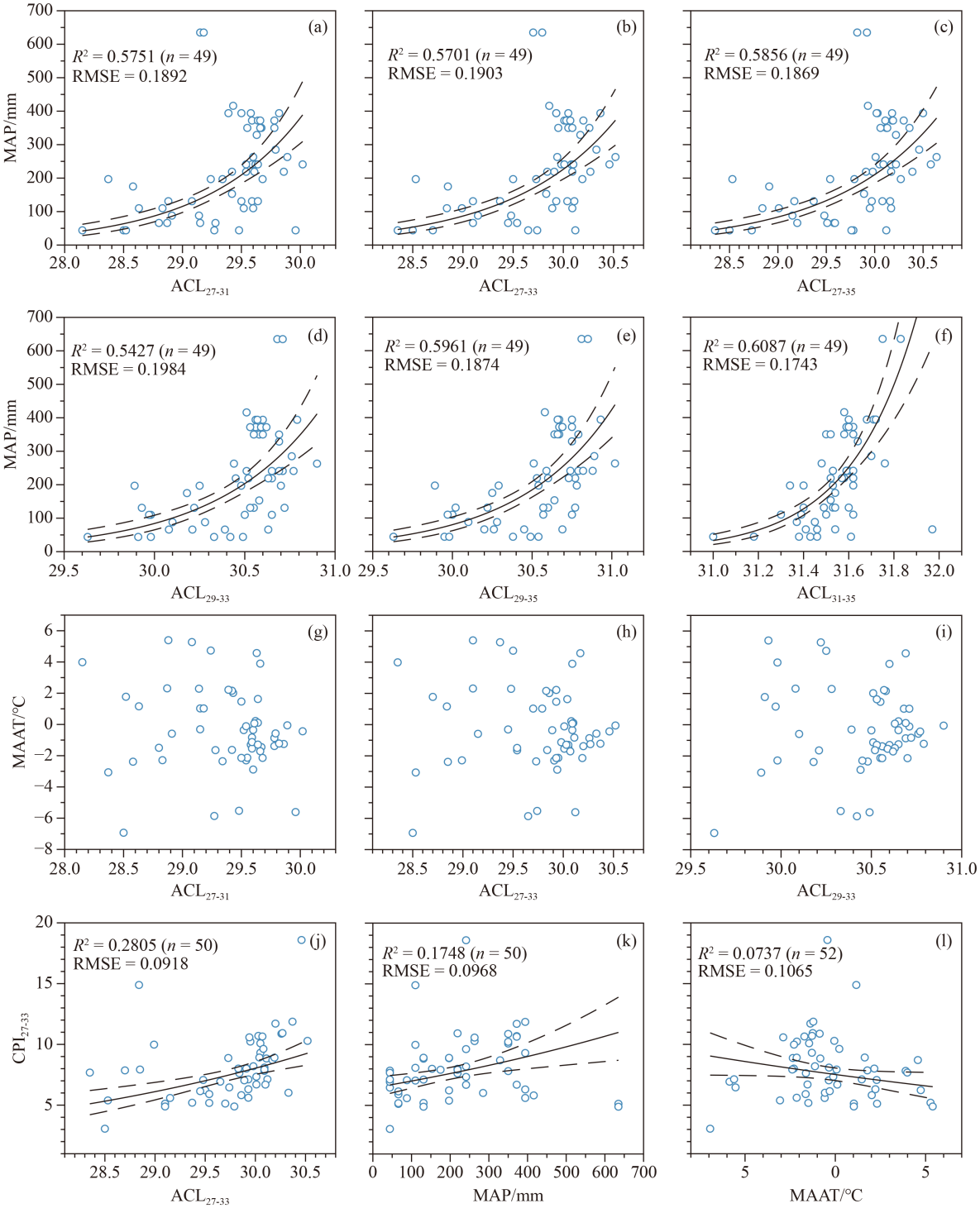


**Fig. 5** Results of exponential regression analysis, showing significant relationships between ACL, CPI, and climatic variables. Outliers were removed before the statistical analyses were performed.

On the other hand, precipitation at our surveyed sites ranges from 44 to 635 mm, while the temperature range is relatively small, reducing the effects of temperature on the long-chain *n*-alkane distributions. A similar interpretation of other biomarkers, including alkenones, was made by Liu et al. (2011) for the lakes across the QTP.

#### 4.3.2 Relationship between ACL and precipitation

Water stress has been shown to induce the production of alkanes with longer chain lengths in leaf wax (Bondada et al., 1996), and that the chain length decreases with increasing precipitation. In our database, ACL is positively correlated with precipitation (Fig. 5), which

contradicts the physiologic stress hypothesis. We speculate that such a relationship is the result of the distinct response of the plants to hydrological changes. Our hypothesis is that plants on the QTP produce higher ACLs in wetter environments. However, in a few cases the data from different plant species have shown a positive but statistically insignificant relationship (Guo et al., 2015). Additionally, to the best of our knowledge, only one case study observed a similar correlation: the plant, *Eucalyptus*, in northern Australia, showed an increase in ACL under wetter conditions (Hoffmann et al., 2013). Clearly, there is a substantial difference in vegetation types between the QTP and Australia, and thus the plants at our sites are unlikely to show a similar response. The cause of the relationship between ACL and the hydrological conditions remains unclear, and next we attempt to examine the potential causes of the observed relationship between ACL and precipitation.

First, we speculate that the cause of a positive relationship between ACL and precipitation is due to the direct impact of hydrological changes on the ACL. A relatively high proportion of long-chain *n*-alkanes from terrestrial higher plants transported to lakes may be supplied by surface runoff. As precipitation increases, the enhanced runoff would cause a greater contribution from land plants to the sedimentary long-chain *n*-alkane pools. Liu and Liu (2016) considered that the contribution of long chain *n*-alkanes to lake sediments from certain aquatic plants may be significant. Aquatic plants have longer than expected chain lengths; for example, some submerged plants contain high concentrations of $C_{27}$ and $C_{29}$ *n*-alkanes. Our PCA results support the previous finding that the $C_{27}$ and $C_{29}$ *n*-alkanes are of mixed origin (Fig. 4). Nevertheless, *n*-alkane chain length distributions are generally different between terrestrial plants and aquatic plants, and therefore higher ACL values reflect a greater contribution from terrestrial plants over aquatic plants. To test this assumption, we compared the correlations between precipitation and ACL with different carbon number ranges, and we observed a similar robust regression relationship for the longer *n*-alkanes (e.g., $ACL_{31\text{-}35}$) (Fig. 5). Therefore, it is unlikely that the cause of the positive correlation between ACL and precipitation is due to the relative contributions of terrestrial and aquatic plants driven by hydrological changes.

Second, we infer that microbial degradation of long-chain *n*-alkanes could account for the unexpected response. Previous investigations found that alkane-degrading microorganisms are widespread in natural environments, and Rojo (2009) pointed out that a typical soil contained significant amounts of hydrocarbon-degrading microorganisms. Alkane-degrading bacteria were also abundant for lake sediments, such as those across the QTP (Wang et al., 2019). Previous findings demonstrated that leaf waxes could potentially undergo microbial degradation during deposition (Zech et al., 2011; Li et al., 2017; Wu et al., 2019a); hence, selective degradation could modify the distributions of long-chain *n*-alkanes during deposition in soils and sediments. We compared the relationships between ACL and precipitation in different types of samples from the early research on the QTP, including for modern plants (Guo et al., 2015), soils (Guo et al., 2015; Jia et al., 2016), and lake sediments (Hu et al., 2014; Ling et al., 2021). We found that the responses of ACL to precipitation were similar in these samples, all showing positive correlations. However, Guo et al. (2015) found that relationship was statistically insignificant for plants and soils, which can be ascribed to the specific habitats for plant growth, such as alpine meadow on the QTP (Dr. Yanjun Guo, personal communication). We infer that the positive correlation between ACL and precipitation may be the result of soil microbial activity. The moisture level is one of the factors that determine the rate of microbial decomposition of organic compounds in soils (Šepič et al., 1995). A higher soil water content caused by higher precipitation may greatly affect soil chemical processes and soil microbial activity, degrading shorter *n*-alkanes in long-chain homologs and leading to higher ACLs. This assumption is supported by the CPI data, which is positively correlated with precipitation (Fig. 5). Overall, we conclude that microbial degradation may play a major role in determining this relationship, but further investigations are needed to elucidate this process.

### 4.4 Implications for lake sediment-based paleoclimate reconstruction across the QTP

ACL changes are considered to reflect climate variables only if the vegetation types remain unchanged during the study period (Hoffmann et al., 2013; Pu et al., 2013). A substantial body of research demonstrates that the vegetation is a major determinant of the chain length of leaf waxes (Vogts et al., 2009); hence, it is imperative to consider the vegetation history over the interval of interest before using the long-chain *n*-alkane ACL as a paleoclimate indicator. Our results reveal that ACL mainly reflects regional climate signals rather than vegetation dynamics. On the other hand, paleovegetation reconstructions have shown that a forest biome was almost absent in most parts of the QTP since the Last Glacial Maximum (Ni et al., 2014; Li et al., 2019; Qin et al., 2022). A spatiotemporal reconstruction of $C_4$ plants also showed that their distribution was less than 10% on the QTP over the past 21000 years (Jiang et al., 2019). Considering the results of the present study and past vegetation reconstructions, we regard the ACL as a proxy for precipitation across most of the QTP, where trees and $C_4$ plants are largely absent.

## 5 Conclusions

We report the distribution of *n*-alkanes extracted from the surface sediments of 55 lakes across the Qinghai-Tibet Plateau. The results show the ACL of the long-chain *n*-alkanes is more responsive to precipitation rather than to temperature in this region. We also found a significant positive relationship between ACL and precipitation, and thus our data support the conclusion that precipitation is the main driver of the variations in ACL. Precipitation changes may affect soil moisture levels and thereby affect microbial degradation. Our results provide new insights into the interpretation of the chain length variability of *n*-alkanes in the lake sediments of the QTP, and they have implications for the use of the *n*-alkane ACL in paleolimnological studies in other high-elevation environments.

**Acknowledgments** We thank Mr. Mohammad Ali Salik from the Biomarkers for Environmental and Climate Science (BECS) research group at the University of Glasgow for assistance with laboratory techniques and equipment, Dr. Feng Qin for discussion of the vegetation information extraction, Dr. Yan Yan for discussion of *n*-alkanes, and Dr. Jan Bloemendal for English language improvement. We are especially grateful to Prof. Xianyu Huang and an anonymous reviewer for their helpful suggestions and advice for improving the manuscript. This work was financially supported by the National Natural Science Foundation of China (Grant No. 42171159) and the Second Tibetan Plateau Scientific Expedition and Research Program (STEP) (No. 2019QZKK0601). Financial support to Mingda Wang for a one-year visit to the University of Glasgow from the Chinese Academy of Sciences is also acknowledged.

**Competing interests** The authors declare that they have no competing interests.

## References

Aichner B, Herzschuh U, Wilkes H (2010). Influence of aquatic macrophytes on the stable carbon isotopic signatures of sedimentary organic matter in lakes on the Tibetan Plateau. Org Geochem, 41(7): 706–718

Badewien T, Vogts A, Rullkötter J (2015). *n*-Alkane distribution and carbon stable isotope composition in leaf waxes of $C_3$ and $C_4$ plants from Angola. Org Geochem, 89–90: 71–79

Bai Y, Azamdzhon M, Wang S, Fang X, Guo H, Zhou P, Chen C, Liu X, Jia S, Wang Q (2019). An evaluation of biological and climatic effects on plant *n*-alkane distributions and $\delta^2H_{alk}$ in a field experiment conducted in central Tibet. Org Geochem, 135: 53–63

Bai Y, Fang X, Nie J, Wang Y, Wu F (2009). A preliminary reconstruction of the paleoecological and paleoclimatic history of the Chinese Loess Plateau from the application of biomarkers. Palaeogeogr Palaeoclimatol Palaeoecol, 271(1–2): 161–169

Bird B W, Polisar P J, Lei Y, Thompson L G, Yao T, Finney B P, Bain D J, Pompeani D P, Steinman B A (2014). A Tibetan lake sediment record of Holocene Indian summer monsoon variability. Earth Planet Sci Lett, 399: 92–102

Bliedtner M, Schäfer I K, Zech R, von Suchodoletz H (2018). Leaf wax *n*-alkanes in modern plants and topsoils from eastern Georgia (Caucasus)–implications for reconstructing regional paleovegetation. Biogeosciences, 15(12): 3927–3936

Bondada B R, Oosterhuis D M, Murphy J B, Kim K S (1996). Effect of water stress on the epicuticular wax composition and ultrastructure of cotton (*Gossypium hirsutum* L.) leaf, bract, and boll. Environ Exp Bot, 36(1): 61–69

Brincat D, Yamada K, Ishiwatari R, Uemura H, Naraoka H (2000). Molecular-isotopic stratigraphy of long-chain *n*-alkanes in Lake Baikal Holocene and glacial age sediments. Org Geochem, 31(4): 287–294

Bush R T, McInerney F A (2013). Leaf wax *n*-alkane distributions in and across modern plants: implications for paleoecology and chemotaxonomy. Geochim Cosmochim Acta, 117: 161–179

Bush R T, McInerney F A (2015). Influence of temperature and $C_4$ abundance on *n*-alkane chain length distributions across the central USA. Org Geochem, 79: 65–73

Callegaro A, Battistel D, Kehrwald N M, Matsubara Pereira F, Kirchgeorg T, Villoslada Hidalgo M D C, Bird B W, Barbante C (2018). Fire, vegetation, and Holocene climate in a southeastern Tibetan lake: a multi-biomarker reconstruction from Paru Co. Clim Past, 14(10): 1543–1563

Carr A S, Boom A, Grimes H L, Chase B M, Meadows M E, Harris A (2014). Leaf wax *n*-alkane distributions in arid zone South African flora: environmental controls, chemotaxonomy and palaeoecological implications. Org Geochem, 67: 72–84

Castañeda I S, Caley T, Dupont L, Kim J H, Malaizé B, Schouten S (2016). Middle to Late Pleistocene vegetation and climate change in subtropical southern East Africa. Earth Planet Sci Lett, 450: 306–316

Castañeda I S, Mulitza S, Schefuss E, Lopes dos Santos R A, Sinninghe Damsté J S, Schouten S (2009a). Wet phases in the Sahara/Sahel region and human migration patterns in North Africa. Proc Natl Acad Sci USA, 106(48): 20159–20163

Castañeda I S, Werne J P, Johnson T C, Filley T R (2009b). Late Quaternary vegetation history of southeast Africa: the molecular isotopic record from Lake Malawi. Palaeogeogr Palaeoclimatol Palaeoecol, 275(1–4): 100–112

Chen L, Zhou W, Zhang Y, Zheng Y, Huang X (2020). Postglacial floral and climate changes in southeastern China recorded by distributions of *n*-alkan-2-ones in the Dahu sediment-peat sequence. Palaeogeogr Palaeoclimatol Palaeoecol, 538: 109448

Chen Y, Cao J, Zhao J, Xu H, Arimoto R, Wang G, Han Y, Shen Z, Li G (2014). *n*-alkanes and polycyclic aromatic hydrocarbons in total suspended particulates from the southeastern Tibetan Plateau: concentrations, seasonal variations, and sources. Sci Total Environ, 470-471: 9–18

Cooper J E, Bray E E (1963). A postulated role of fatty acids in petroleum formation. Geochim Cosmochim Acta, 27(11): 1113–1127

Diefendorf A F, Freeman K H, Wing S L, Graham H V (2011). Production of *n*-alkyl lipids in living plants and implications for the geologic past. Geochim Cosmochim Acta, 75(23): 7472–7485

Dodd R S, Afzal-Rafii Z (2000). Habitat-related adaptive properties of plant cuticular lipids. Evolution, 54(4): 1438–1444

Dodd R S, Poveda M M (2003). Environmental gradients and population divergence contribute to variation in cuticular wax composition in *Juniperus communis*. Biochem Syst Ecol, 31(11): 1257–1270

Doskey P V (2000). The air–water exchange of $C_{15}$–$C_{31}$ *n*-alkanes in a precipitation-dominated seepage lake. Atmos Environ, 34(23): 3981–3993

Duan Y I, He J (2011). Distribution and isotopic composition of *n*-alkanes from grass, reed and tree leaves along a latitudinal gradient in China. Geochem J, 45(3): 199–207

Eglinton G, Hamilton R J (1967). Leaf epicuticular waxes. Science, 156(3780): 1322–1335

Eley Y L, Hren M T (2018). Reconstructing vapor pressure deficit from leaf wax lipid molecular distributions. Sci Rep, 8(1): 3967

Feakins S J, deMenocal P B, Eglinton T I (2005). Biomarker records of late Neogene changes in northeast African vegetation. Geology, 33(12): 977–980

Freeman K H, Pancost R D (2014). Biomarkers for terrestrial plants and climate. In: Holland HD, Turekian K K, eds. Treatise on Geochemistry. Oxford: Elsevier

Gagosian R B, Peltzer E T (1986). The importance of atmospheric input of terrestrial organic material to deep sea sediments. Org Geochem, 10(4–6): 661–669

Gaines S M, Eglinton G, Rullkötter J (2009). Echoes of life: what fossil molecules reveal about Earth history. Now York: Oxford University Press

Garcin Y, Schefuß E, Schwab V F, Garreta V, Gleixner G, Vincens A, Todou G, Séné O, Onana J M, Achoundong G, Sachse D (2014). Reconstructing $C_3$ and $C_4$ vegetation cover using *n*-alkane carbon isotope ratios in recent lake sediments from Cameroon, Western Central Africa. Geochim Cosmochim Acta, 142: 482–500

Gong P, Wang X, Yao T (2011). Ambient distribution of particulate- and gas-phase *n*-alkanes and polycyclic aromatic hydrocarbons in the Tibetan Plateau. Environ Earth Sci, 64(7): 1703–1711

Günther F, Thiele A, Biskop S, Mäusbacher R, Haberzettl T, Yao T, Gleixner G (2016). Late quaternary hydrological changes at Tangra Yumco, Tibetan Plateau: a compound-specific isotope-based quantification of lake level changes. J Paleolimnol, 55(4): 369–382

Guo Y, Guo N, He Y, Gao J (2015). Cuticular waxes in alpine meadow plants: climate effect inferred from latitude gradient in Qinghai-Tibetan Plateau. Ecol Evol, 5(18): 3954–3968

Häggi C, Eglinton T I, Zech W, Sosin P, Zech R (2019). A 250 ka leaf-wax $\delta$D record from a loess section in Darai Kalon, Southern Tajikistan. Quat Sci Rev, 208: 118–128

He J, Yang K, Tang W, Lu H, Qin J, Chen Y, Li X (2020). The first high-resolution meteorological forcing dataset for land process studies over China. Sci Data, 7(1): 25

Hockun K, Mollenhauer G, Ho S L, Hefter J, Ohlendorf C, Zolitschka B, Mayr C, Lücke A, Schefuß E (2016). Using distributions and stable isotopes of *n*-alkanes to disentangle organic matter contributions to sediments of Laguna Potrok Aike, Argentina. Org Geochem, 102: 110–119

Hoffmann B, Kahmen A, Cernusak L A, Arndt S K, Sachse D (2013). Abundance and distribution of leaf wax *n*-alkanes in leaves of Acacia and Eucalyptus trees along a strong humidity gradient in northern Australia. Org Geochem, 62: 62–67

Hollister K V, Thomas E K, Raynolds M K, Bültmann H, Raberg J H, Miller G H, Sepúlveda J (2022). Aquatic and terrestrial plant contributions to sedimentary plant waxes in a modern Arctic lake setting. J Geophys Res: Biogeosci, 127: e2022JG006903

Hou X (2001). Vegetation Atlas of China. Beijing: Science Press

Howard S, McInerney F A, Caddy-Retalic S, Hall P A, Andrae J W (2018). Modelling leaf wax *n*-alkane inputs to soils along a latitudinal transect across Australia. Org Geochem, 121: 126–137

Hu X, Zhu L, Wang Y, Wang J, Peng P, Ma Q, Hu J, Lin X (2014). Climatic significance of *n*-alkanes and their compound-specific $\delta$D values from lake surface sediments on the southwestern Tibetan Plateau. Chin Sci Bull, 59(24): 3022–3033

Huang Y, Freeman K H, Eglinton T I, Alayne Street-Perrott F (1999a). $\delta^{13}$C analyses of individual lignin phenols in Quaternary lake sediments: a novel proxy for deciphering past terrestrial vegetation changes. Geology, 27(5): 471–474

Huang Y, Street-Perrott F A, Perrott R A, Metzger P, Eglinton G (1999b). Glacial–interglacial environmental changes inferred from molecular and compound-specific $\delta^{13}$C analyses of sediments from Sacred Lake, Mt. Kenya. Geochim Cosmochim Acta, 63(9): 1383–1404

Immerzeel W W, Lutz A F, Andrade M, Bahl A, Biemans H, Bolch T, Hyde S, Brumby S, Davies B J, Elmore A C, Emmer A, Feng M, Fernández A, Haritashya U, Kargel J S, Koppes M, Kraaijenbrink P D A, Kulkarni A V, Mayewski P A, Nepal S, Pacheco P, Painter T H, Pellicciotti F, Rajaram H, Rupper S, Sinisalo A, Shrestha A B, Viviroli D, Wada Y, Xiao C, Yao T, Baillie J E M (2020). Importance and vulnerability of the world's water towers. Nature, 577(7790): 364–369

Immerzeel W W, van Beek L P, Bierkens M F (2010). Climate change will affect the Asian water towers. Science, 328(5984): 1382–1385

Jalali B, Sicre M A, Kallel N, Azuara J, Combourieu-Nebout N, Bassetti M A, Klein V (2017). High-resolution Holocene climate and hydrological variability from two major Mediterranean deltas (Nile and Rhone). Holocene, 27(8): 1158–1168

Jia Q, Sun Q, Xie M, Shan Y, Ling Y, Zhu Q, Tian M (2016). Normal alkane distributions in soil samples along a Lhasa-Bharatpur Transect. Acta Geol Sin, 90: 738–748

Jiang W, Wu H, Li Q, Lin Y, Yu Y (2019). Spatiotemporal changes in $C_4$ plant abundance in China since the Last Glacial Maximum and their driving factors. Palaeogeogr Palaeoclimatol Palaeoecol, 518: 10–21

Jin C, Günther F, Li S, Jia G, Peng P, Gleixner G (2016). Reduced early Holocene moisture availability inferred from $\delta$D values of sedimentary *n*-alkanes in Zigetang Co, Central Tibetan Plateau. Holocene, 26(4): 556–566

Ju J T, Zhu L P, Huang L, Yang R M, Ma Q F, Hu X, Wang Y J, Zhen X L (2015). Ranwu Lake, a proglacial lake with the potential to reflect glacial activity in SE Tibet. Chin Sci Bull, 60(1): 16–26 (in Chinese)

Kawamura K, Ishimura Y, Yamazaki K (2003). Four years' observations of terrestrial lipid class compounds in marine aerosols from the western North Pacific. Global Biogeochem Cycles, 17: 3–1-3–19

Kuechler R R, Schefuß E, Beckmann B, Dupont L, Wefer G (2013). NW African hydrology and vegetation during the Last Glacial cycle reflected in plant-wax-specific hydrogen and carbon isotopes. Quat Sci Rev, 82: 56–67

Kusch S, Rethemeyer J, Schefuß E, Mollenhauer G (2010). Controls on the age of vascular plant biomarkers in Black Sea sediments. Geochim Cosmochim Acta, 74(24): 7031–7047

Leider A, Hinrichs K U, Schefuß E, Versteegh G J M (2013). Distribution and stable isotopes of plant wax derived *n*-alkanes in lacustrine, fluvial and marine surface sediments along an Eastern Italian transect and their potential to reconstruct the hydrological cycle. Geochim Cosmochim Acta, 117: 16–32

Li L, Li Q, Li J, Wang H, Dong L, Huang Y, Wang P (2015). A hydroclimate regime shift around 270ka in the western tropical Pacific inferred from a late Quaternary *n*-alkane chain-length record. Palaeogeogr Palaeoclimatol Palaeoecol, 427: 79–88

Li Q, Wu H, Yu Y, Sun A, Luo Y (2019). Large-scale vegetation history in China and its response to climate change since the Last Glacial Maximum. Quat Int, 500: 108–119

Li R, Fan J, Xue J, Meyers P A (2017). Effects of early diagenesis on molecular distributions and carbon isotopic compositions of leaf wax long chain biomarker *n*-alkanes: comparison of two one-year-long burial experiments. Org Geochem, 104: 8–18

Ling Y, Sun Q, Zheng M, Wang H, Luo Y, Dai X, Xie M, Zhu Q (2017a). Alkenone-based temperature and climate reconstruction during the last deglaciation at Lake Dangxiong Co, southwestern Tibetan Plateau. Quat Int, 443: 58–69

Ling Y, Zheng M, Sun Q, Dai X (2017b). Last deglacial climatic variability in Tibetan Plateau as inferred from *n*-alkanes in a sediment core from Lake Zabuye. Quat Int, 454: 15–24

Ling Y, Zheng M, Wang S, Sun Q, Xie B, Zhang C (2021). The impact of climatic and environmental factors on *n*-alkanes indices in southwestern Tibetan Plateau. Acta Geol Sin, 95: 648–658

Liu H, Liu W (2016). *n*-Alkane distributions and concentrations in algae, submerged plants and terrestrial plants from the Qinghai-Tibetan Plateau. Org Geochem, 99: 10–22

Liu J, Shen Z, Chen W, Chen J, Zhang X, Chen J, Chen F (2021). Dipolar mode of precipitation changes between north China and the Yangtze River Valley existed over the entire Holocene: evidence from the sediment record of Nanyi Lake. Int J Climatol, 41(3): 1667–1681

Liu W, Liu Z, Wang H, He Y, Wang Z, Xu L (2011). Salinity control on long-chain alkenone distributions in lake surface waters and sediments of the northern Qinghai-Tibetan Plateau, China. Geochim Cosmochim Acta, 75(7): 1693–1703

Liu W, Yang H, Wang H, An Z, Wang Z, Leng Q (2015). Carbon isotope composition of long chain leaf wax *n*-alkanes in lake sediments: a dual indicator of paleoenvironment in the Qinghai-Tibet Plateau. Org Geochem, 83–84: 190–201

Liu X, Cheng Z, Yan L, Yin Z Y (2009). Elevation dependency of recent and future minimum surface air temperature trends in the Tibetan Plateau and its surroundings. Global Planet Change, 68(3): 164–174

McDuffee K E, Eglinton T I, Sessions A L, Sylva S, Wagner T, Hayes J M (2004). Rapid analysis of $^{13}C$ in plant-wax *n*-alkanes for reconstruction of terrestrial vegetation signals from aquatic sediments. Geochem Geophys Geosyst, 5(10): Q10004

Meyers P A (1997). Organic geochemical proxies of paleoceanographic, paleolimnologic, and paleoclimatic processes. Org Geochem, 27(5–6): 213–250

Meyers P A, Ishiwatari R (1995). Organic matter accumulation records in lake sediments. In: Lerman A, Imboden D M, Gat J R, eds. Physics and Chemistry of Lakes. Heidelberg: Springer Berlin

Mountain Research Initiative EDW Working Group (2015). Elevation-dependent warming in mountain regions of the world. Nat Clim Chang, 5(5): 424–430

Naafs B D A, Inglis G N, Blewett J, McClymont E L, Lauretano V, Xie S, Evershed R P, Pancost R D (2019). The potential of biomarker proxies to trace climate, vegetation, and biogeochemical processes in peat: a review. Global Planet Change, 179: 57–79

Nelson D B, Ladd S N, Schubert C J, Kahmen A (2018). Rapid atmospheric transport and large-scale deposition of recently synthesized plant waxes. Geochim Cosmochim Acta, 222: 599–617

Ni J, Cao X, Jeltsch F, Herzschuh U (2014). Biome distribution over the last 22,000yr in China. Palaeogeogr Palaeoclimatol Palaeoecol, 409: 33–47

Nichols J E, Booth R K, Jackson S T, Pendall E G, Huang Y (2006). Paleohydrologic reconstruction based on *n*-alkane distributions in ombrotrophic peat. Org Geochem, 37(11): 1505–1513

Norström E, Katrantsiotis C, Smittenberg R H, Kouli K (2017). Chemotaxonomy in some Mediterranean plants and implications for fossil biomarker records. Geochim Cosmochim Acta, 219: 96–110

Norström E, Neumann F H, Scott L, Smittenberg R H, Holmstrand H, Lundqvist S, Snowball I, Sundqvist H S, Risberg J, Bamford M (2014). Late Quaternary vegetation dynamics and hydro-climate in the Drakensberg, South Africa. Quat Sci Rev, 105: 48–65

Norström E, Norén G, Smittenberg R H, Massuanganhe E A, Ekblom A (2018). Leaf wax $\delta$D inferring variable medieval hydroclimate and early initiation of Little Ice Age (LIA) dryness in southern Mozambique. Global Planet Change, 170: 221–233

Poynter J G, Farrimond P, Robinson N, Eglinton G (1989). Aeolian-derived higher plant lipids in the marine sedimentary record: links with palaeoclimate. In: Leinen M, Sarnthein M, eds. Paleoclimatology and Paleometeorology: Modern and Past Patterns of Global Atmospheric Transport. Dordrecht: Springer

Poynter J, Eglinton G (1990). Molecular composition of three sediments from Hole 717 C: the Bengal fan. In: Proceedings of the Ocean Drilling Program, Scientific Results, 155–161

Pu Y, Nace T, Meyers P A, Zhang H, Wang Y, Zhang C L, Shao X (2013). Paleoclimate changes of the last 1000 yr on the eastern Qinghai–Tibetan Plateau recorded by elemental, isotopic, and molecular organic matter proxies in sediment from glacial Lake Ximencuo. Palaeogeogr Palaeoclimatol Palaeoecol, 379–380: 39–53

Qiao B, Zhu L, Yang R (2019). Temporal-spatial differences in lake water storage changes and their links to climate change throughout the Tibetan Plateau. Remote Sens Environ, 222: 232–243

Qin F (2021). Modern pollen assemblages of the surface lake sediments from the steppe and desert zones of the Tibetan Plateau. Sci China Earth Sci, 64(3): 425–439

Qin F, Zhao Y, Cao X (2022). Biome reconstruction on the Tibetan Plateau since the Last Glacial Maximum using a machine learning method. Sci China Earth Sci, 65(3): 518–535

Rao Z, Jia G, Qiang M, Zhao Y (2014). Assessment of the difference between mid- and long chain compound specific $\delta$D-alkanes values in lacustrine sediments as a paleoclimatic indicator. Org Geochem, 76: 104–117

Rao Z, Zhu Z, Jia G, Chen F, Barton L, Zhang J, Qiang M (2010). Relationship between climatic conditions and the relative abundance of modern $C_3$ and $C_4$ plants in three regions around the North Pacific. Chin Sci Bull, 55(18): 1931–1936

Rojo F (2009). Degradation of alkanes by bacteria. Environ Microbiol, 11(10): 2477–2490

Rommerskirchen F, Plader A, Eglinton G, Chikaraishi Y, Rullkötter J (2006). Chemotaxonomic significance of distribution and stable carbon isotopic composition of long-chain alkanes and alkan-1-ols in $C_4$ grass waxes. Org Geochem, 37(10): 1303–1332

Sachse D, Billault I, Bowen G J, Chikaraishi Y, Dawson T E, Feakins S J, Freeman K H, Magill C R, McInerney F A, van der Meer M T J, Polissar P, Robins R J, Sachs J P, Schmidt H L, Sessions A L, White J W C, West J B, Kahmen A (2012). Molecular paleohydrology: interpreting the hydrogen-isotopic composition of lipid biomarkers from photosynthesizing organisms. Annu Rev Earth Planet Sci, 40(1): 221–249

Saini J, Günther F, Aichner B, Mischke S, Herzschuh U, Zhang C, Mäusbacher R, Gleixner G (2017). Climate variability in the past ~19,000 yr in NE Tibetan Plateau inferred from biomarker and stable isotope records of Lake Donggi Cona. Quat Sci Rev, 157: 129–140

Sarkar S, Prasad S, Wilkes H, Riedel N, Stebich M, Basavaiah N, Sachse D (2015). Monsoon source shifts during the drying mid-Holocene: biomarker isotope based evidence from the core 'monsoon zone' (CMZ) of India. Quat Sci Rev, 123: 144–157

Schefuß E, Ratmeyer V, Stuut J B W, Jansen J H F, Sinninghe Damsté J S (2003). Carbon isotope analyses of *n*-alkanes in dust from the lower atmosphere over the central eastern Atlantic. Geochim Cosmochim Acta, 67(10): 1757–1767

Šepič E Leskovšek H, Trier C (1995). Aerobic bacterial degradation of selected polyaromatic compounds and *n*-alkanes found in petroleum. J Chromatogr A, 697(1–2): 515–523

Shepherd T, Wynne Griffiths D (2006). The effects of stress on plant cuticular waxes. New Phytol, 171(3): 469–499

Simoneit B R T, Chester R, Eglinton G (1977). Biogenic lipids in particulates from the lower atmosphere over the eastern Atlantic. Nature, 267(5613): 682–685

Sinninghe Damsté J S, Verschuren D, Ossebaar J, Blokker J, van Houten R, van der Meer M T J, Plessen B, Schouten S (2011). A 25,000-year record of climate-induced changes in lowland vegetation of eastern equatorial Africa revealed by the stable carbon-isotopic composition of fossil plant leaf waxes. Earth Planet Sci Lett, 302(1–2): 236–246

Still C J, Berry J A, Collatz G J, Defries R S (2009). ISLSCP, II: $C_4$ (Vegetation Percentage. In. ORNL Distributed Active Archive Center)

Still C J, Berry J A, Collatz G J, DeFries R S (2003). Global distribution of $C_3$ and $C_4$ vegetation: carbon cycle implications. Global Biogeochemical Cycles, 17: 6–1-6–14

Sun H, Bendle J, Seki O, Zhou A (2018). Mid- to- late Holocene hydroclimatic changes on the Chinese Loess Plateau: evidence from *n*-alkanes from the sediments of Tianchi Lake. J Paleolimnol, 60(4): 511–523

Tian L, Wang M, Zhang X, Yang X, Zong Y, Jia G, Zheng Z, Man M (2019). Synchronous change of temperature and moisture over the past 50 ka in subtropical southwest China as indicated by biomarker records in a crater lake. Quat Sci Rev, 212: 121–134

Tipple B J, Pagani M (2013). Environmental control on eastern broadleaf forest species' leaf wax distributions and D/H ratios. Geochim Cosmochim Acta, 111: 64–77

Toney J L, García-Alix A, Jiménez-Moreno G, Anderson R S, Moossen H, Seki O (2020). New insights into Holocene hydrology and temperature from lipid biomarkers in western Mediterranean alpine wetlands. Quat Sci Rev, 240: 106395

Vogts A, Moossen H, Rommerskirchen F, Rullkötter J (2009). Distribution patterns and stable carbon isotopic composition of alkanes and alkan-1-ols from plant waxes of African rain forest and savanna $C_3$ species. Org Geochem, 40(10): 1037–1054

Wakeham S G (1996). Aliphatic and polycyclic aromatic hydrocarbons in Black Sea sediments. Mar Chem, 53(3–4): 187–205

Wan W, Long D, Hong Y, Ma Y, Yuan Y, Xiao P, Duan H, Han Z, Gu X (2016). A lake data set for the Tibetan Plateau from the 1960s, 2005, and 2014. Sci Data, 3(1): 1–13

Wang B, Ma Y, Su Z, Wang Y, Ma W (2020). Quantifying the evaporation amounts of 75 high-elevation large dimictic lakes on the Tibetan Plateau. Sci Adv, 6(26): eaay8558

Wang B, Yang J, Jiang H, Zhang G, Dong H (2019). Chemical composition of n-alkanes and microbially mediated *n*-alkane degradation potential differ in the sediments of Qinghai-Tibetan lakes with different salinity. Chem Geol, 524: 37–48

Wang J, Axia E, Xu Y, Wang G, Zhou L, Jia Y, Chen Z, Li J (2018a). Temperature effect on abundance and distribution of leaf wax *n*-alkanes across a temperature gradient along the 400 mm isohyet in China. Org Geochem, 120: 31–41

Wang J, Xu Y, Zhou L, Shi M, Axia E, Jia Y, Chen Z, Li J, Wang G (2018b). Disentangling temperature effects on leaf wax *n*-alkane traits and carbon isotopic composition from phylogeny and precipitation. Org Geochem, 126: 13–22

Wang L, Lü H, Wu N, Chu D, Han J, Wu Y, Wu H, Gu Z (2004). Discovery of $C_4$ species at high altitude in Qinghai-Tibetan Plateau. Chin Sci Bull, 49(13): 1392–1396

Wang M, Zhang W, Hou J (2015). Is average chain length of plant lipids a potential proxy for vegetation, environment and climate changes? Biogeosciences Discuss, 12: 5477–5501

Wang R Z (2003). $C_4$ plants in the vegetation of Tibet, China: their natural occurrence and altitude distribution pattern. Photosynthetica, 41(1): 21–26

Wang S, Dou H (1998). Lakes in China. Beijing: Science Press

Witt R, Günther F, Lauterbach S, Kasper T, Mäusbacher R, Yao T, Gleixner G (2016). Biogeochemical evidence for freshwater periods during the Last Glacial Maximum recorded in lake sediments from Nam Co, south-central Tibetan Plateau. J Paleolimnol, 55(1): 67–82

Wu M S, West A J, Feakins S J (2019a). Tropical soil profiles reveal the fate of plant wax biomarkers during soil storage. Org Geochem, 128: 1–15

Wu Y, Guo L, Zheng H, Zhang B, Li M (2019b). Hydroclimate assessment of gridded precipitation products for the Tibetan Plateau. Sci Total Environ, 660: 1555–1564

Xie M, Sun Q, Dong H, Liu S, Shang W, Ling Y, Zhao J, Chu G (2020). *n*-Alkanes and compound carbon isotope records from Lake Yiheshariwusu in the Hulun Buir sandy land, northeastern China. Holocene, 30(10): 1451–1461

Yan T, He J, Wang Z, Zhang C, Feng X, Sun X, Leng C, Zhao C (2020). Glacial fluctuations over the last 3500 years reconstructed from a lake sediment record in the northern Tibetan Plateau. Palaeogeogr Palaeoclimatol Palaeoecol, 544: 109597

Yao T, Xue Y, Chen D, Chen F, Thompson L, Cui P, Koike T, Lau W K M, Lettenmaier D, Mosbrugger V, Zhang R, Xu B, Dozier J, Gillespie T, Gu Y, Kang S, Piao S, Sugimoto S, Ueno K, Wang L, Wang W, Zhang F, Sheng Y, Guo W, Ailikun, Yang X, Ma Y, Shen S S P, Su Z, Chen F, Liang S, Liu Y, Singh V P, Yang K, Yang D, Zhao X, Qian Y, Zhang Y, Li Q (2019). Recent Third Pole's rapid warming accompanies cryospheric melt and water cycle intensification and interactions between monsoon and environment: multidisciplinary approach with observations, modeling, and analysis. Bull Am Meteorol Soc, 100(3): 423–444

Yokoyama Y, Naruse T, Ogawa N O, Tada R, Kitazato H, Ohkouchi N (2006). Dust influx reconstruction during the last 26000 years inferred from a sedimentary leaf wax record from the Japan Sea. Global Planet Change, 54(3–4): 239–250

Zech M, Pedentchouk N, Buggle B, Leiber K, Kalbitz K, Marković S B, Glaser B (2011). Effect of leaf litter degradation and seasonality on D/H isotope ratios of *n*-alkane biomarkers. Geochim Cosmochim Acta, 75(17): 4917–4928

Zech R, Zech M, Marković S, Hambach U, Huang Y (2013). Humid glacials, arid interglacials? Critical thoughts on pedogenesis and paleoclimate based on multi-proxy analyses of the loess–paleosol sequence Crvenka, Northern Serbia Palaeogeogr Palaeoclimatol Palaeoecol, 387: 165–175

Zhang X, Xu B, Günther F, Witt R, Wang M, Xie Y, Zhao H, Li J, Gleixner G (2017). Rapid northward shift of the Indian Monsoon on the Tibetan Plateau at the end of the Little Ice Age. J Geophys Res Atmos, 122(17): 9262–9279

Zhang Y, Liu X, Lin Q, Gao C, Wang J, Wang G (2014). Vegetation and climate change over the past 800 years in the monsoon margin of northeastern China reconstructed from *n*-alkanes from the Great Hinggan Mountain ombrotrophic peat bog. Org Geochem, 76: 128–135

Zhang Z, Zhao M, Eglinton G, Lu H, Huang C (2006). Leaf wax lipids as paleovegetational and paleoenvironmental proxies for the Chinese Loess Plateau over the last 170 kyr. Quat Sci Rev, 25(5–6): 575–594

Zhao J, Thomas E K, Yao Y, DeAraujo J, Huang Y (2018). Major increase in winter and spring precipitation during the Little Ice Age in the westerly dominated northern Qinghai-Tibetan Plateau. Quat Sci Rev, 199: 30–40

Zhou B, Zheng H, Yang W, Taylor D, Lu Y, Wei G, Li L, Wang H (2012). Climate and vegetation variations since the LGM recorded by biomarkers from a sediment core in the northern South China Sea. J Quaternary Sci, 27(9): 948–955

Zhou W, Xie S, Meyers P A, Zheng Y (2005). Reconstruction of late glacial and Holocene climate evolution in southern China from geolipids and pollen in the Dingnan peat sequence. Org Geochem, 36(9): 1272–1284

Zhou W, Zheng Y, Meyers P A, Jull A J T, Xie S (2010). Postglacial climate-change record in biomarker lipid compositions of the Hani peat sequence, northeastern China. Earth Planet Sci Lett, 294(1–2): 37–46

Zhu C S, Li L J, Huang H, Dai W T, Lei Y L, Qu Y, Huang R J, Wang Q Y, Shen Z X, Cao J J (2020). *n*-Alkanes and PAHs in the southeastern Tibetan Plateau: characteristics and correlations with brown carbon light absorption. J Geophys Res: Atmos, 125: e2020JD032666